Search for stable hadronizing squarks and gluinos in e^+e^- collisions up to $\sqrt{s} = 209\,\mathrm{GeV}$

The ALEPH Collaboration*)

Abstract

Searches for stable, hadronizing scalar quarks and gluinos are performed using the data collected with the ALEPH detector at LEP. Gluon splitting into a gluino or a squark pair is searched for at centre-of-mass energies around the Z resonance, in the $e^+e^- \to q\bar{q}\tilde{g}\tilde{g}$ and $q\bar{q}\tilde{q}\bar{\tilde{q}}$ processes. Stable squark pair production, and stop pair production with subsequent decays into a stable gluino, $\tilde{t} \to c\tilde{g}$, are also directly searched for at centre-of-mass energies from 183 to 209 GeV.

Altogether, stable hadronizing stop (sbottom) quarks are excluded up to masses of 95 (92) GeV/c^2, and stable hadronizing gluinos are excluded up to 26.9 GeV/c^2, at 95% confidence level. In the framework of R-parity-conserving supersymmetric models in which the gluino and the stop quark are the two lightest supersymmetric particles, a 95% C.L. lower limit of 80 GeV/c^2 is set on the stop quark mass.

---

*) See next pages for the list of authors

The ALEPH Collaboration

A. Heister, S. Schael

  Physikalisches Institut das RWTH-Aachen, D-52056 Aachen, Germany

R. Barate, R. Brunelière, I. De Bonis, D. Decamp, C. Goy, S. Jezequel, J.-P. Lees, F. Martin, E. Merle, M.-N. Minard, B. Pietrzyk, B. Trocmé

  Laboratoire de Physique des Particules (LAPP), IN^{2}P^3-CNRS, F-74019 Annecy-le-Vieux Cedex, France

S. Bravo, M.P. Casado, M. Chmeissani, J.M. Crespo, E. Fernandez, M. Fernandez-Bosman, Ll. Garrido,[15] M. Martinez, A. Pacheco, H. Ruiz

  Institut de Física d'Altes Energies, Universitat Autònoma de Barcelona, E-08193 Bellaterra (Barcelona), Spain[7]

A. Colaleo, D. Creanza, N. De Filippis, M. de Palma, G. Iaselli, G. Maggi, M. Maggi, S. Nuzzo, A. Ranieri, G. Raso,[24] F. Ruggieri, G. Selvaggi, L. Silvestris, P. Tempesta, A. Tricomi,[3] G. Zito

  Dipartimento di Fisica, INFN Sezione di Bari, I-70126 Bari, Italy

X. Huang, J. Lin, Q. Ouyang, T. Wang, Y. Xie, R. Xu, S. Xue, J. Zhang, L. Zhang, W. Zhao

  Institute of High Energy Physics, Academia Sinica, Beijing, The People's Republic of China[8]

D. Abbaneo, T. Barklow,[26] O. Buchmüller,[26] M. Cattaneo, B. Clerbaux,[23] H. Drevermann, R.W. Forty, M. Frank, F. Gianotti, J.B. Hansen, J. Harvey, D.E. Hutchcroft,[30], P. Janot, B. Jost, M. Kado,[2] P. Mato, A. Moutoussi, F. Ranjard, L. Rolandi, D. Schlatter, G. Sguazzoni, F. Teubert, A. Valassi, I. Videau

  European Laboratory for Particle Physics (CERN), CH-1211 Geneva 23, Switzerland

F. Badaud, S. Dessagne, A. Falvard,[20] D. Fayolle, P. Gay, J. Jousset, B. Michel, S. Monteil, D. Pallin, J.M. Pascolo, P. Perret

  Laboratoire de Physique Corpusculaire, Université Blaise Pascal, IN^{2}P^3-CNRS, Clermont-Ferrand, F-63177 Aubière, France

J.D. Hansen, J.R. Hansen, P.H. Hansen, A.C. Kraan, B.S. Nilsson

  Niels Bohr Institute, 2100 Copenhagen, DK-Denmark[9]

A. Kyriakis, C. Markou, E. Simopoulou, A. Vayaki, K. Zachariadou

  Nuclear Research Center Demokritos (NRCD), GR-15310 Attiki, Greece

A. Blondel,[12] J.-C. Brient, F. Machefert, A. Rougé, H. Videau

  Laoratoire Leprince-Ringuet, Ecole Polytechnique, IN^{2}P^3-CNRS, F-91128 Palaiseau Cedex, France

V. Ciulli, E. Focardi, G. Parrini

  Dipartimento di Fisica, Università di Firenze, INFN Sezione di Firenze, I-50125 Firenze, Italy

A. Antonelli, M. Antonelli, G. Bencivenni, F. Bossi, G. Capon, F. Cerutti, V. Chiarella, P. Laurelli, G. Mannocchi,[5] G.P. Murtas, L. Passalacqua

  Laboratori Nazionali dell'INFN (LNF-INFN), I-00044 Frascati, Italy

J. Kennedy, J.G. Lynch, P. Negus, V. O'Shea, A.S. Thompson

  Department of Physics and Astronomy, University of Glasgow, Glasgow G12 8QQ,United Kingdom[10]

S. Wasserbaech

  Utah Valley State College, Orem, UT 84058, U.S.A.

R. Cavanaugh,[4] S. Dhamotharan,[21] C. Geweniger, P. Hanke, V. Hepp, E.E. Kluge, A. Putzer, H. Stenzel, K. Tittel, M. Wunsch[19]

Kirchhoff-Institut für Physik, Universität Heidelberg, D-69120 Heidelberg, Germany[16]

R. Beuselinck, W. Cameron, G. Davies, P.J. Dornan, M. Girone,[1] R.D. Hill, N. Marinelli, J. Nowell, S.A. Rutherford, J.K. Sedgbeer, J.C. Thompson,[14] R. White

Department of Physics, Imperial College, London SW7 2BZ, United Kingdom[10]

V.M. Ghete, P. Girtler, E. Kneringer, D. Kuhn, G. Rudolph

Institut für Experimentalphysik, Universität Innsbruck, A-6020 Innsbruck, Austria[18]

E. Bouhova-Thacker, C.K. Bowdery, D.P. Clarke, G. Ellis, A.J. Finch, F. Foster, G. Hughes, R.W.L. Jones, M.R. Pearson, N.A. Robertson, M. Smizanska

Department of Physics, University of Lancaster, Lancaster LA1 4YB, United Kingdom[10]

O. van der Aa, C. Delaere,[28] G.Leibenguth,[31] V. Lemaitre[29]
Institut de Physique Nucléaire, Département de Physique, Université Catholique de Louvain, 1348 Louvain-la-Neuve, Belgium

U. Blumenschein, F. Hölldorfer, K. Jakobs, F. Kayser, K. Kleinknecht, A.-S. Müller, B. Renk, H.-G. Sander, S. Schmeling, H. Wachsmuth, C. Zeitnitz, T. Ziegler

Institut für Physik, Universität Mainz, D-55099 Mainz, Germany[16]

A. Bonissent, P. Coyle, C. Curtil, A. Ealet, D. Fouchez, P. Payre, A. Tilquin
Centre de Physique des Particules de Marseille, Univ Méditerranée, IN^{2}P^3-CNRS, F-13288 Marseille, France

F. Ragusa
Dipartimento di Fisica, Università di Milano e INFN Sezione di Milano, I-20133 Milano, Italy.

A. David, H. Dietl, G. Ganis,[27] K. Hüttmann, G. Lütjens, W. Männer, H.-G. Moser, R. Settles, M. Villegas, G. Wolf

Max-Planck-Institut für Physik, Werner-Heisenberg-Institut, D-80805 München, Germany[16]

J. Boucrot, O. Callot, M. Davier, L. Duflot, J.-F. Grivaz, Ph. Heusse, A. Jacholkowska,[6] L. Serin, J.-J. Veillet
Laboratoire de l'Accélérateur Linéaire, Université de Paris-Sud, IN^{2}P^3-CNRS, F-91898 Orsay Cedex, France

P. Azzurri, G. Bagliesi, T. Boccali, L. Foà, A. Giammanco, A. Giassi, F. Ligabue, A. Messineo, F. Palla, G. Sanguinetti, A. Sciabà, P. Spagnolo R. Tenchini A. Venturi P.G. Verdini
Dipartimento di Fisica dell'Università, INFN Sezione di Pisa, e Scuola Normale Superiore, I-56010 Pisa, Italy

O. Awunor, G.A. Blair, G. Cowan, A. Garcia-Bellido, M.G. Green, L.T. Jones, T. Medcalf, A. Misiejuk, J.A. Strong, P. Teixeira-Dias
Department of Physics, Royal Holloway & Bedford New College, University of London, Egham, Surrey TW20 OEX, United Kingdom[10]

R.W. Clifft, T.R. Edgecock, P.R. Norton, I.R. Tomalin, J.J. Ward
Particle Physics Dept., Rutherford Appleton Laboratory, Chilton, Didcot, Oxon OX11 OQX, United Kingdom[10]

B. Bloch-Devaux, D. Boumediene, P. Colas, B. Fabbro, E. Lançon, M.-C. Lemaire, E. Locci, P. Perez, J. Rander, B. Tuchming, B. Vallage
CEA, DAPNIA/Service de Physique des Particules, CE-Saclay, F-91191 Gif-sur-Yvette Cedex, France[17]

A.M. Litke, G. Taylor
Institute for Particle Physics, University of California at Santa Cruz, Santa Cruz, CA 95064, USA[22]

C.N. Booth, S. Cartwright, F. Combley,[25] P.N. Hodgson, M. Lehto, L.F. Thompson

Department of Physics, University of Sheffield, Sheffield S3 7RH, United Kingdom[10]

A. Böhrer, S. Brandt, C. Grupen, J. Hess, A. Ngac, G. Prange

Fachbereich Physik, Universität Siegen, D-57068 Siegen, Germany[16]

C. Borean, G. Giannini

Dipartimento di Fisica, Università di Trieste e INFN Sezione di Trieste, I-34127 Trieste, Italy

H. He, J. Putz, J. Rothberg

Experimental Elementary Particle Physics, University of Washington, Seattle, WA 98195 U.S.A.

S.R. Armstrong, K. Berkelman, K. Cranmer, D.P.S. Ferguson, Y. Gao,[13] S. González, O.J. Hayes, H. Hu, S. Jin, J. Kile, P.A. McNamara III, J. Nielsen, Y.B. Pan, J.H. von Wimmersperg-Toeller, W. Wiedenmann, J. Wu, Sau Lan Wu, X. Wu, G. Zobernig

Department of Physics, University of Wisconsin, Madison, WI 53706, USA[11]

G. Dissertori

Institute for Particle Physics, ETH Hönggerberg, 8093 Zürich, Switzerland.

1 Introduction

A search for squark production in e^+e^- collisions is relevant at LEP energies because the stop quark and, to a lesser extent, the sbottom quark, could well be the lightest supersymmetric partner of all standard model fermions [1].

Searches for squarks have already been performed by ALEPH [2, 3] in the framework of the MSSM, the minimal supersymmetric extension of the standard model [4], with R-parity conservation and the assumption that the lightest supersymmetric particle (LSP) is the lightest neutralino or the sneutrino. These searches yielded an absolute lower limit on the stop mass of $63\,\mathrm{GeV}/c^2$ at the 95% confidence level.

This absolute lower limit does not apply if the LSP is either the gluino or the squark itself. Supersymmetric models in which the gluino is the LSP are reviewed in Ref. [5]. Squarks as LSP's are cosmologically disfavoured because of their nonzero electric charge [6], but could be sufficiently stable to behave like the LSP in the LEP detectors. Scenarios in which the gluino is the next-to-lightest supersymmetric particle (NLSP) and decays into a b quark and a long-lived sbottom (with mass 2 to $5\,\mathrm{GeV}/c^2$) have been proposed to explain excesses in $b\bar{b}$ production at hadron colliders [7].

In this paper, it is assumed that the LSP is either the gluino or a squark, in the context of the MSSM with R-parity conservation. Under this assumption, the NLSP would decay with a 100% branching fraction into the LSP, e.g., $\tilde{t} \rightarrow c\tilde{g}$, $\tilde{b} \rightarrow b\tilde{g}$ or $\tilde{g} \rightarrow \tilde{b}\bar{b}$. (Stop decays into $t\tilde{g}$ and gluino decays into $\tilde{t}\bar{t}$ can only happen for stop and gluino masses larger than the top quark mass, which is beyond the reach of LEP.) This coloured LSP is stable and hadronizes into stable, colourless, charged and neutral bound states. These bound states (e.g., $\tilde{g}g$, $\tilde{g}q\bar{q}$, $\tilde{g}qqq$, $\tilde{q}\bar{q}$, $\tilde{q}qq$) are called R-hadrons, in which "R" refers to the fact that they carry one unit of R-parity [8].

An important consequence is that the missing energy signature might not automatically be present, in contrast to other searches for supersymmetric particles in which the LSP is a weakly-interacting particle, i.e., a neutralino or a sneutrino. However, when the LSP is sufficiently heavy, the maximum energy available for R-hadronic interactions turns out to be quite small. Indeed, the centre-of-mass energy E_{scat} of the R-hadronic interaction with ordinary matter, made of nucleons of mass m_{N}, is very close to the mass m_{R} of the R-hadron, almost independently of the R-hadron energy E_{R}: $E_{\mathrm{scat}}^2 = m_{\mathrm{R}}^2 + m_{\mathrm{N}}^2 + 2m_{\mathrm{N}}E_{\mathrm{R}}$. It leaves little energy ($E_{\mathrm{scat}} - m_{\mathrm{R}} - m_{\mathrm{N}}$) for each R-hadronic interaction in the calorimeters. For example, for $m_{\mathrm{R}} = 50\,\mathrm{GeV}/c^2$ and $E_{\mathrm{R}} = 90\,\mathrm{GeV}$, this energy amounts to $800\,\mathrm{MeV}$, to be compared to $\sim 12\,\mathrm{GeV}$ for a pion of the same energy.

Because of this reduced hadronic interaction, a large missing energy signal is expected from heavy neutral R-hadrons. Heavy charged R-hadrons are expected to interact mostly electromagnetically like heavy muons. Searches for missing energy and for stable heavy charged particles are therefore well suited to look for stable squarks and gluinos.

In view of covering all possible configurations in the plane ($m_{\tilde{g}}$, $m_{\tilde{q}}$) with a squark or a gluino LSP (or, equivalently, with a long-lived squark or gluino), the processes investigated in this paper are

1. the $e^+e^- \rightarrow q\bar{q}\tilde{g}\tilde{g}$ process, with a gluon splitting into a pair of stable gluinos;

2. the $e^+e^- \to q\bar{q}\tilde{q}\bar{\tilde{q}}$ process, with a gluon splitting into a pair of stable squarks;

3. the pair production of stable squarks, $e^+e^- \to \tilde{t}\bar{\tilde{t}}$ and $\tilde{b}\bar{\tilde{b}}$;

4. the stop pair production with decays into stable gluinos, $e^+e^- \to \tilde{t}\bar{\tilde{t}} \to c\tilde{g}\bar{c}\tilde{g}$.

The first two processes were searched for using the data collected by ALEPH at LEP 1, at centre-of-mass energies around the Z resonance. These data correspond to about 4.5 million hadronic Z decays. The data collected at LEP 2 were used to analyse the last two processes. The integrated luminosities and centre-of-mass energies of these data are indicated in Table 1.

Table 1: Integrated luminosities, centre-of-mass energy ranges and mean centre-of-mass energy values for the data collected during the years 1997-2000.

Year	Luminosity [pb^{-1}]	Energy range [GeV]	$\langle\sqrt{s}\rangle$ [GeV]
2000	9.4	207-209	208.0
	122.6	206-207	206.6
	75.3	204-206	205.2
1999	42.0	-	201.6
	86.2	-	199.5
	79.8	-	195.5
	28.9	-	191.6
1998	173.6	-	188.6
1997	56.8	-	182.7

This paper is organized as follows. The detector is briefly described in Section 2. The simulation of the signal final states is discussed in detail in Section 3, and a brief account of the simulation of the standard model backgrounds is given. The $e^+e^- \to q\bar{q}\tilde{g}\tilde{g}$ and $q\bar{q}\tilde{q}\bar{\tilde{q}}$ searches at LEP 1 are presented in Sections 4 and 5, followed by the search for stable squark pair production at LEP 2 in Section 6, and by the search for decaying stop quarks in Section 7. The result of the combination of all these analyses is given in Section 8.

2 The ALEPH detector

A detailed description of the ALEPH detector and of its performance can be found in Refs. [9, 10]. Only a summary is given here.

Charged particles are detected in the central part, consisting of a precision silicon vertex detector, a cylindrical drift chamber and a large time projection chamber, which measure altogether up to 31 space points along the charged particle trajectories. The time projection chamber also provides 359 measurements (338 from wires and 21 from pads) of the specific energy loss by ionization dE/dx. A 1.5 T axial magnetic field is provided by a superconducting solenoidal coil. Charged particle transverse momenta are reconstructed

with a $1/p_T$ resolution of $6 \times 10^{-4} \oplus 5 \times 10^{-3}/p_T$ (p_T in GeV/c). In the following, *good tracks* are defined as charged particle tracks reconstructed with at least four hits in the time projection chamber, originating from within a cylinder of length $20\,\mathrm{cm}$ and radius $2\,\mathrm{cm}$ coaxial with the beam and centred at the nominal collision point, and with a polar angle with respect to the beam such that $|\cos\theta| < 0.95$.

Electrons and photons are identified by the characteristic longitudinal and transverse developments of the associated showers in the electromagnetic calorimeter, a 22 radiation length thick sandwich of lead planes and proportional wire chambers with fine read-out segmentation. The relative energy resolution achieved is $0.18/\sqrt{E}$ (E in GeV) for isolated electrons and photons.

Muons are identified by their characteristic penetration pattern in the hadron calorimeter, a 1.5 m thick yoke interleaved with 23 layers of streamer tubes, together with two surrounding double-layers of muon chambers. In association with the electromagnetic calorimeter, the hadron calorimeter also provides a measurement of the hadronic energy with a relative resolution of $0.85/\sqrt{E}$ (E in GeV).

The total visible energy, and therefore the missing energy, is measured with an energy-flow reconstruction algorithm which combines all the above measurements, supplemented by the energy detected down to $34\,\mathrm{mrad}$ from the beam axis ($24\,\mathrm{mrad}$ at LEP 1) by two additional electromagnetic calorimeters, used for the luminosity determination. The relative resolution on the total visible energy is $0.60/\sqrt{E}$ (E in GeV) for high-multiplicity final states. This algorithm also provides a list of reconstructed objects, classified as charged particles, photons and neutral hadrons, called *energy-flow particles* in the following, and used to determine the event characteristics for the selections presented in this paper.

3 Monte Carlo Simulation

3.1 Signal simulation

3.1.1 Production processes

The simulation of squark pair production at LEP 2 energies was performed with the `PYTHIA` event generator [11]. For the simulation of gluon splitting into a gluino pair at the Z resonance, the program mentioned in Ref. [5] was used, modified to include initial-state radiation as described in Ref. [12] and to generate events as in Ref. [13]. The QCD leading-order production cross section for $e^+e^- \rightarrow q\bar{q}\tilde{g}\tilde{g}$ was determined numerically with this program, and cross-checked with the analytical predictions of Refs. [14, 15], after proper quark to gluino colour-factor modification. These analytical formulae also allowed the $e^+e^- \rightarrow q\bar{q}\tilde{q}\bar{\tilde{q}}$ cross section to be determined, by appropriately modifying the quark to a squark phase space factor. The calculation of the resummed QCD next-to-leading-order cross section for gluon splitting into a gluino or a squark pair was performed following the prescriptions of Ref. [15], with the running of the strong coupling constant corrected for the presence of a light gluino or a light squark [16]. The resulting Z partial widths are displayed in Fig. 1 as a function of the gluino and the squark mass.
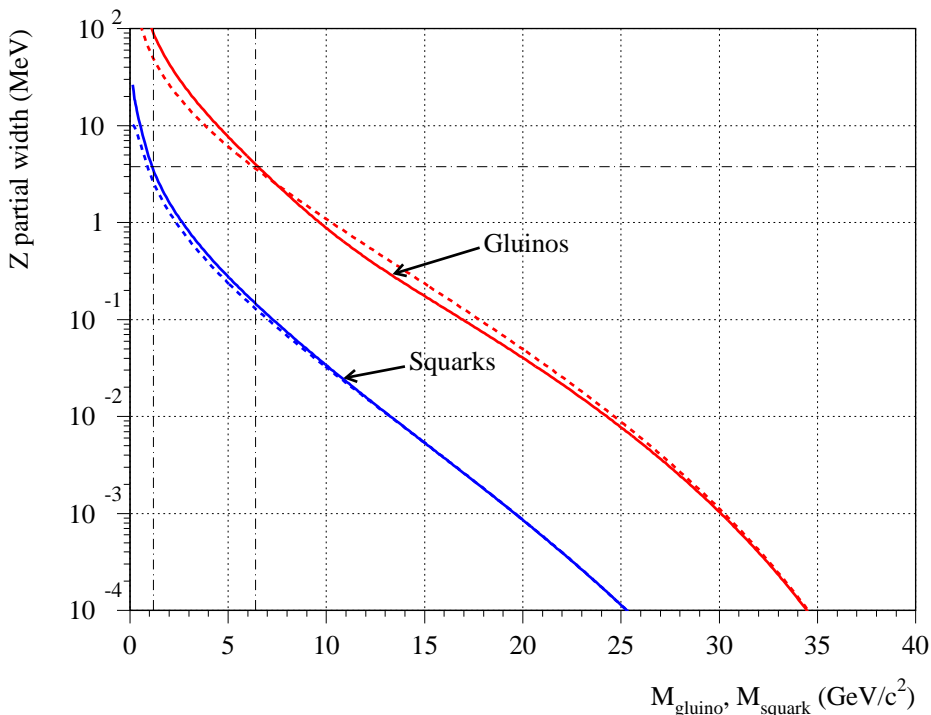
Figure 1: The Z → q̄q̃g̃ and Z → q̄q̃q̃̄ partial widths as a function of the squark and the gluino mass, computed at the leading order (dashed curves) and resummed at the next-to-leading order (full curves). Also shown are the corresponding 95% C.L. lower limits on the squark and gluino masses when the contribution to the Z width exceeds 3.9 MeV (Ref. [17] and Section 4).

3.1.2 R-hadron formation

The hadronization of the (s)partons generated as described above was done with `PYTHIA`. Because squark and gluino hadronization is not available by default, `PYTHIA` had to be extended with a few dedicated routines [18]. The following issues are addressed therein.

Stable gluino and squark hadronization   Stable gluinos and squarks are allowed to radiate gluons [19] as any other coloured particles. The fragmentation is handled with a Peterson function [20] with a parameter extrapolated [21] from its value for b quarks:

$$\frac{\epsilon_{\tilde{q},\tilde{g}}}{\epsilon_b} = \frac{m_b^2}{m_{\tilde{q},\tilde{g}}^2}. \tag{1}$$

However, a gluino is attached to two, rather than one, string pieces. In this case, the fragmentation is applied to each of the two pieces, thereby giving a larger energy loss than for a (s)quark.

Both R-meson and R-baryon production are possible. All R-hadrons made of a given squark or gluino are assumed to be equal in mass, with an electric charge of −1, 0 or 1, determined by the quark and squark content. The relative fractions of charged and neutral R-hadrons are then obtained by simple statistics, and are typically half and half, except for gluino R-hadrons, for which the additional possibility to form a gluino-gluon bound state enhances the fraction of neutral R-hadrons by an unknown amount.

In the processes studied in this paper, R-hadrons are produced in pairs, so that double neutral (R^0R^0), mixed ($R^0R^\pm$) or double charged ($R^\pm R^\pm, R^\pm R^\mp$) final states are possible. There is no significant correlation between the electric charges of the two gluino R-hadrons. Charge conservation is ensured by the presence of additional fragmentation particles in the final state.

Stop-hadron decay   The stop decay to c$\tilde{g}$ proceeds through loop diagrams or through unlikely FCNC tree-level couplings [22], which leads to a lifetime larger than the typical hadronization time. The stop quark therefore hadronizes into a stop R-hadron before decaying. The decay is described in the framework of the spectator model [23], in which the bound state quarks act as spectators to the decaying stop.

3.1.3   R-hadronic interaction in the calorimeters

A major issue of the simulation is the treatment of the interaction of R-hadrons in the detector. Extensive studies have been done on this subject [5, 24]. The simple approach chosen here to simulate R-hadronic interactions, in analogy with Ref. [3], is to treat R-hadrons as heavy pions in the `GHEISHA` package (in which the hadron mass is properly accounted for), with the modification that the low energy pion-nucleon resonances are removed.

3.1.4   Free parameters

Several unknown parameters, listed below, are needed to fully specify the R-hadron phenomenology, and may be the source of sizeable systematic uncertainties.

- The probability $P_{\tilde{g}g}$ to form a gluon-gluino bound state. This quantity is essentially unknown and can vary between 0 and 1. For $P_{\tilde{g}g} = 0$, the fractions of double neutral, mixed and double charged final states are approximately 25%, 50%, and 25%, respectively. In the configuration in which $P_{\tilde{g}g} = 1$ (unlikely for gluino masses in excess of $25\,\mathrm{GeV}/c^2$ [5, 24]), only purely neutral final states are produced.

- The effective spectator mass $M_{\mathrm{spec}}^{\mathrm{eff}}$ of squark and gluino R-hadrons. It roughly corresponds to the difference between the constituent mass and the current algebra mass. The value obtained from hadron mass spectroscopy is $M_{\mathrm{spec}}^{\mathrm{eff}} = 0.5^{+0.5}_{-0.2}\,\mathrm{GeV}/c^2$ [25].

- The gluon constituent mass $M_{\mathrm{g}}^{\mathrm{c}}$. Its value is estimated from glueball searches [26] to be $M_{\mathrm{g}}^{\mathrm{c}} = 0.7^{+0.3}_{-0.4}\,\mathrm{GeV}/c^2$, to be compared to the quark constituent mass, typically twice smaller.

- The total cross section σ_{RN} of R-hadron-nucleon scattering. It is assumed to be equal to the cross section $\sigma_{\pi\mathrm{N}}$ of pion-nucleon scattering because *(i)* at high momentum, the interaction cross section of any hadron on a nucleon is proportional to the sum of the individual valence parton cross sections, and *(ii)* heavy partons (with a mass above a couple of GeV/c^2) do no interact significantly. The sum therefore

runs only over the standard partons, in which each quark accounts for one unit of cross section, and each colour octet gluon for 9/4 units. For gluinos, the R-meson ($\tilde{g}q\bar{q}$) hadronic cross section is thus equal to that of a pion, the $\tilde{g}g$ bound state cross section is $9/4/(1+1) = 9/8$ larger, and the R-baryon ($\tilde{g}qqq$) cross section is $(1+1+1)/(1+1) = 3/2$ larger. For squark-R-mesons ($\tilde{q}\bar{q}$), the same argument yields a ratio of $1/2$ while, for squark-R-baryons ($\tilde{q}qq$), the ratio is equal to unity. Altogether, it is therefore reasonable to use an average R-hadronic interaction cross section identical to that of pions, with an uncertainty of $\pm 50\%$.

3.1.5 Simulated signal samples

In order to design the signal selection criteria, hundreds of simulated signal samples of 1000 to 4000 events each were generated for each of the four processes mentioned in Section 1. Gluon splitting to gluino or squark pairs was simulated for gluino/squark masses between 0 and $40\,\text{GeV}/c^2$, with a typical step of $2\,\text{GeV}/c^2$. For squark pair production, samples with squark and gluino masses ranging from 0 to $90\,\text{GeV}/c^2$ with a typical $5\,\text{GeV}/c^2$ step were generated, with two values of the squark mixing angle: *(i)* $0°$ and *(ii)* the value for which the squark coupling to the Z vanishes, *i.e.*, $56°$ for stops and $68°$ for sbottoms.

3.2 Background simulation

Simulated samples for all relevant standard model background processes were generated both at LEP 1 and LEP 2 energies. Bhabha scattering was simulated with the `BHWIDE` generator [27]. The `KORALZ` package [28] was used for the other difermion processes. Two-photon interactions were simulated with `PHOT02` [29]. The W^+W^- production was simulated with `KORALW` [30], the production of $We\nu$ with `GRC4F` [31] and the Zee, ZZ and $Z\nu\bar{\nu}$ final states with `PYTHIA` [32].

4 Search for $e^+e^- \rightarrow q\bar{q}\tilde{g}\tilde{g}$ with LEP 1 data

At LEP 1, events resulting from gluon radiation off a $q\bar{q}$ pair, with subsequent gluon splitting into two stable gluinos, are expected to show as a pair of acoplanar jets, accompanied by two stable R-hadrons.

When the gluino mass is small, the $e^+e^- \rightarrow q\bar{q}\tilde{g}\tilde{g}$ production cross section is large enough to sizeably contribute to the Z hadronic width. The accurate electroweak measurements at LEP and SLC allow a model-independent upper limit of $3.9\,\text{MeV}$ to be set on the Z width for purely hadronic final states [17]. All gluino masses below $6.3\,\text{GeV}/c^2$ are therefore excluded at the 95% confidence level [17], as can be seen in Fig. 1, irrespective of the gluino decay and hadronization mechanisms. For larger masses, the final state topology, and therefore the search strategy, depends on the electric charges of the R-hadrons.

4.1 Search for two neutral R-hadrons

When the two R-hadrons are neutral, the acoplanar jet pair is accompanied by missing energy arising from the specific interaction of massive neutral R-hadrons with the detector. The acoplanar jet selection developed for the $H\nu\bar{\nu}$ search [33] may therefore be used. Its efficiency reaches $\sim 9\%$ for $m_{\tilde{g}} = 25\,\mathrm{GeV}/c^2$, as is visible from the dashed curve in Fig. 2. This analysis was optimized for the case of a heavy Higgs boson, leading to non-violently acoplanar hadronic jets and a moderate, but isolated, missing energy, which makes it inadequate for gluino masses above 30 and below $15\,\mathrm{GeV}/c^2$.
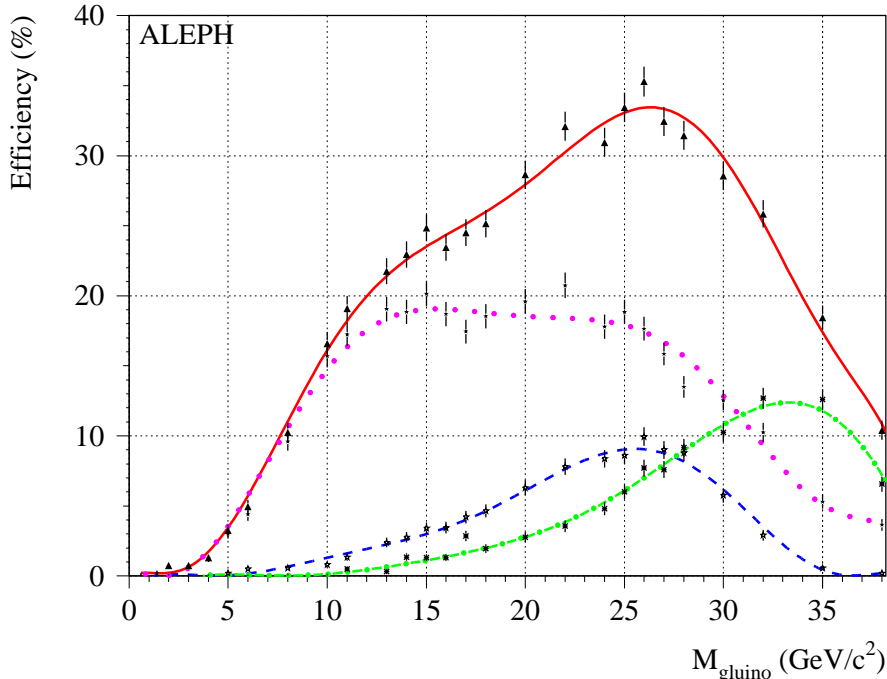

Figure 2: The $q\bar{q}\tilde{g}\tilde{g}$ selection efficiency as a function of the gluino mass, for the $H\nu\bar{\nu}$ selection (dashed curve), the additional efficiency of the large-mass selection (dot-dashed curve), the additional efficiency of the small-mass selection (dotted curve), and the sum of the three (full curve). The markers with error bars indicate the efficiencies obtained with each of the simulated samples, and the curves are obtained with a polynomial fit through these points.

4.1.1 Large gluino masses

For gluino masses above $30\,\mathrm{GeV}/c^2$, the missing energy and the jet acoplanarity become so large that simpler and, in this configuration, more efficient selection criteria can be designed with the same topological variables as in the $H\nu\bar{\nu}$ search. Such selection criteria were optimized for a search for the stop quark [34], and are summarized below.

Only events with at least four good tracks are considered. Most of the $q\bar{q}$ background is rejected by the requirement that the visible mass be smaller than $50\%\sqrt{s}$. Events with a small angle θ_{T} of the thrust axis with respect to the beam ($\cos\theta_{\mathrm{T}} > 0.9$) are eliminated, and so are events with energy detected within $12°$ from the beam axis, to avoid events in which energy escapes down the beam pipe. The bulk of two-photon interactions is rejected by requiring that the total momentum transverse to the beam exceed $5\%\sqrt{s}$.

For events with at least eight good tracks (mostly q$\bar{\text{q}}$ events), the acollinearity and the acoplanarity angles are required to be smaller than 135° and 150°, respectively. Three-jet events with one energetic neutrino from heavy-quark semi-leptonic decays are rejected by requiring that the total momentum transverse to the beam remain smaller than 30 GeV/c. To reject three-jet events with two such neutrinos, the aplanarity (*i.e.*, the sum of the three jet-jet angles when the event is forced to form three jets) has to be less than 350°.

In events with less than eight good tracks, the thrust axis angle with respect to the beam axis has to be larger than 45°. For monojet events, *i.e.*, events in which one hemisphere (with respect to a plane perpendicular to the thrust axis) is empty, it is further required that the visible mass be in excess of 5 GeV/c^2 and the thrust smaller than 0.95. These cuts eliminate the two-photon interactions and the e$^+$e$^- \to \tau^+\tau^-$ background. For non-monojet events, each hemisphere must contain at least two good tracks and the acoplanarity angle has to be less than 150°, which rejects the remaining $\tau^+\tau^-$ background.

The additional efficiency brought by this large-mass selection exceeds 10% for $m_{\tilde{\text{g}}}$ above 30 GeV/c^2, as can be seen from the dot-dashed curve in Fig. 2.

4.1.2 Small gluino masses

For gluino masses below 15 GeV/c^2, the R-hadrons tend to interact more in the calorimeters, and a third jet, mostly formed with neutral hadronic energy, develops around the still large missing energy. Requirements like missing energy isolation or substantial aplanarity therefore become inefficient, and must be replaced by more selective criteria aimed at this specific three-jet topology.

Only hadronic events (more than five good tracks carrying more than 10% of the centre-of-mass energy) with a visible mass smaller than 65 GeV/c^2 are considered here. As in the H$\nu\bar{\nu}$ selection, the acollinearity and the acoplanarity angles are required to be less than 165° and 175°, respectively. Similarly, events with less than 75% of the visible energy above 30° from the beam axis are eliminated, and so are the events with any activity below 12°. Two-photon interactions are rejected by requiring that the missing transverse momentum exceed 5%$\sqrt{s}$ for events with a visible mass below 20 GeV/c^2, and that the missing momentum point more than 35° away from the beam axis. The latter cut also rejects q$\bar{\text{q}}$ events with an undetected, energetic, initial-state-radiation photon.

The remaining events are then forced to form three jets with the Durham algorithm. To ensure a three-jet topology, the values where the transitions from three to two jets (y_{23}) and to four jets (y_{34}) occur are required to exceed 0.01 and to be less than 0.04, respectively.

To select signal-like events, the "R-hadron jet" candidate, *i.e.*, the jet with the smallest amount of charged energy, is required to contain mostly neutral hadrons, by imposing that its charged energy be smaller than 20% of its neutral hadronic energy. (The latter is computed as the energy sum of all neutral energy-flow particles in the jet with a hadron calorimeter component.) Because the missing energy is also expected to point in the direction of the "R-hadron jet" candidate, it is finally required that the amount of charged energy in a cone of 35° around the missing momentum direction be smaller than 3 GeV. As can be inferred from Fig. 3, these last two criteria cut the expected background by a factor larger than a thousand, but only reduce the signal efficiency by a modest 30%.
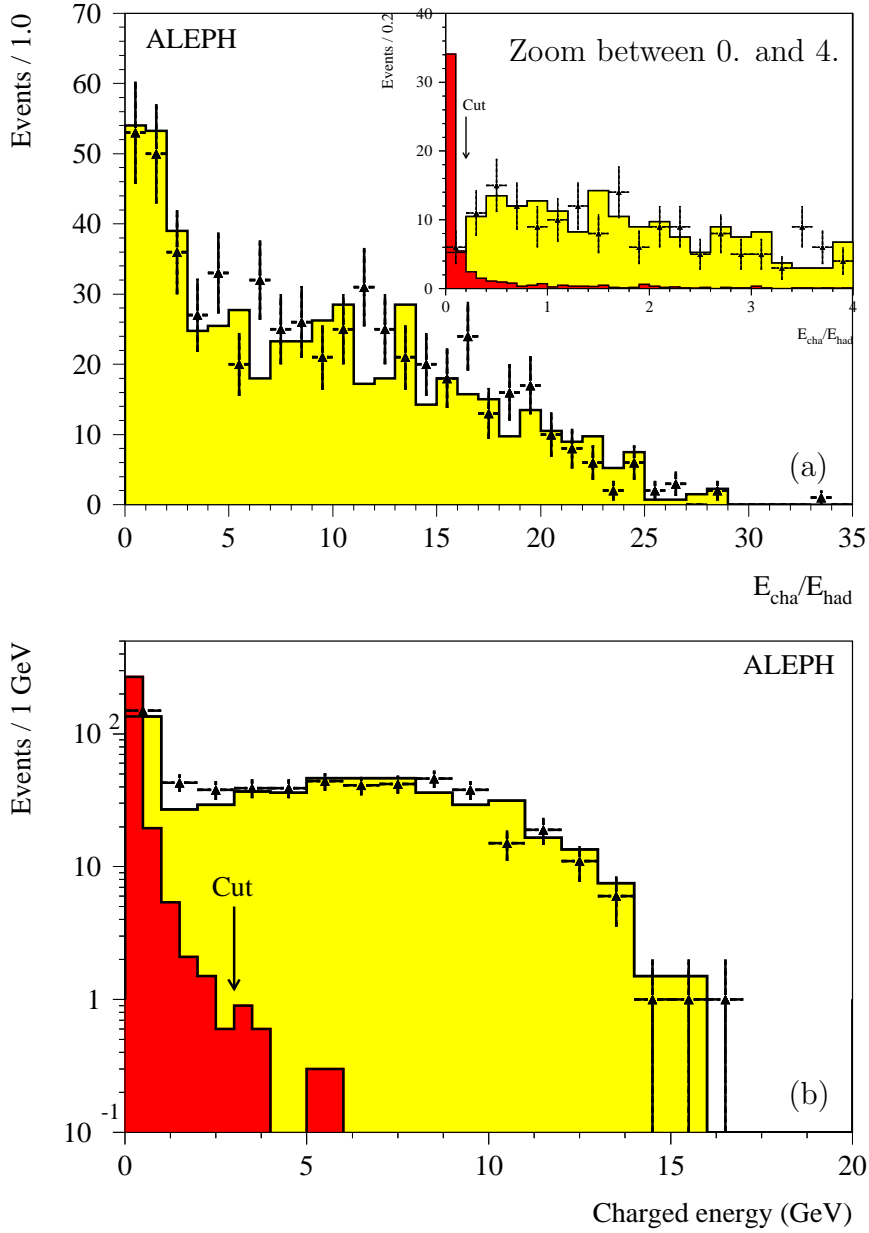
Figure 3: Distributions of (a) the ratio of the "R-hadron jet" charged energy to its neutral hadronic energy; and (b) the charged energy in a $35°$ cone around the missing momentum, before the corresponding cuts are applied, for the data (triangles with error bars), the background simulation (light-shaded histogram) and the signal with $m_{\tilde{g}} = 10\,\text{GeV}/c^2$ (dark-shaded histogram, arbitrary normalization).

The additional efficiency brought by this last selection is shown by the dotted curve in Fig. 2. As anticipated, the selection is well suited for masses around $15\,\text{GeV}/c^2$ and below. Although not specifically designed for large masses, the selection also contributes substantially all the way up to $40\,\text{GeV}/c^2$.

When the three searches are combined, the $q\bar{q}R^0R^0$ selection efficiency exceeds 15% for masses between 10 and $35\,\text{GeV}/c^2$, and culminates at about 35% for $m_{\tilde{g}} = 27\,\text{GeV}/c^2$. It decreases fast for small gluino masses but it does not completely vanish, even for

massless gluinos. Indeed, when two energetic light neutral R-hadrons are produced, they are expected to be detected as normal neutral hadrons in the hadron calorimeter. Due to calorimeter resolution effects, this large neutral hadronic energy occasionally causes sizeable missing energy and acoplanarity.

No events were selected in the data in either of the three selections, with an expected background of less than two events at 95% confidence level.

4.2 Search for charged R-hadrons

If the probability $P_{\tilde{g}g}$ to form a gluon-gluino bound state is not 100%, a relevant fraction of the final states contains one or two charged R-hadrons (up to 75% for $P_{\tilde{g}g} = 0$). These heavy stable charged particles can be identified with their isolation from the rest of the event, as well as their unusual energy loss by ionization in the time projection chamber.

Events with at least five good tracks are considered in this search. Heavy stable charged particle track candidates must be reconstructed with at least half of the 338 wires and the 21 pads of the time projection chamber, must have a momentum larger than $2.5\,\mathrm{GeV}/c$, and must be isolated from the other good tracks of the event by more than $18.2°$. To ensure a reliable momentum determination, the track-fit-χ^2 probability is required to exceed 1%. The energy loss by ionization is then required to be at least three standard deviations away from that expected for light stable charged particles (electrons, muons, pions, kaons or protons) of the same momentum. After this preselection, a total of 364 events with at least one heavy stable charged particle track candidate is selected from the data, in agreement with the 363 ± 16 events expected. The distribution of N_σ, the number of standard deviations with respect to the ionization expected in the most-likely light-particle hypothesis, is displayed in Fig. 4a, and that of the cosine of the isolation angle in Fig. 4b. A reasonable agreement is observed between the data and the simulation in both variables. In particular, the dE/dx distribution of very ionizing particles (mostly alpha particles) is well reproduced by the simulation.

The distributions of N_σ as a function of the track candidate momentum are shown in Fig. 4c for the data, and in Fig. 4d for signal events with different gluino masses. Events with two heavy stable charged particle track candidates are kept as $q\bar{q}R^\pm R^\pm$ candidates. Events with only one such track, *i.e.*, $q\bar{q}R^\pm R^0$ candidates, are required to have a visible mass smaller than $75\,\mathrm{GeV}/c^2$, to account for the presence of a neutral R-hadron. The track candidate must also satisfy one of the two following tightened identification criteria in order to reject the remaining background:

(i) either the track is isolated from the other good tracks of the event by more than $25.8°$ and its fit-χ^2 probability is in excess of 10%, in which case its energy loss by ionization is required to be at least four standard deviations away from that expected for light stable charged particles of the same momentum;

(ii) or its momentum is larger than $5\,\mathrm{GeV}/c$, in which case the energy loss by ionization is required to be *smaller* than expected for light charged particles.
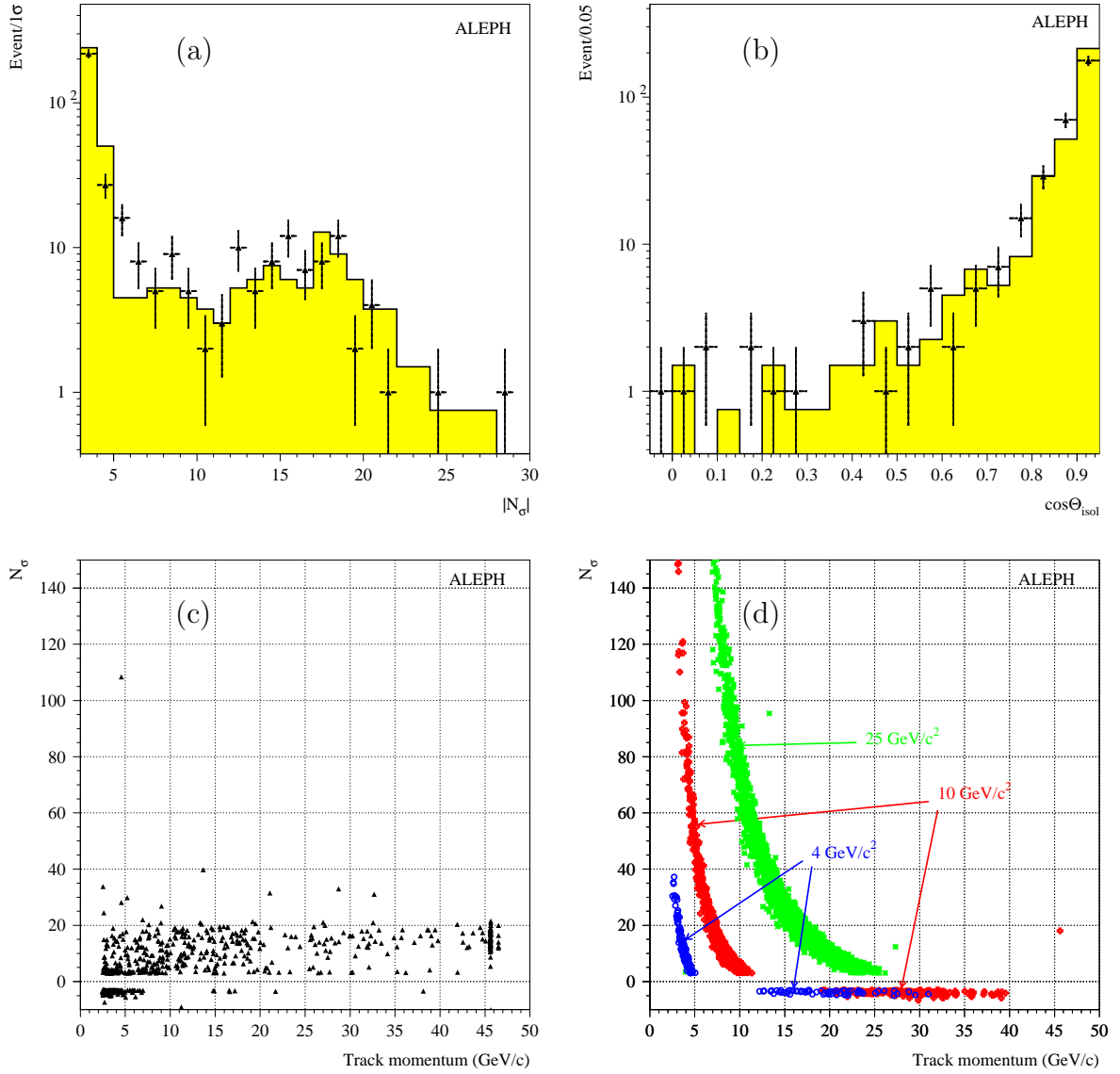
Figure 4: Distributions of (a) $|N_\sigma|$, the number of standard deviations with respect to the expected dE/dx for the most-likely light-particle hypothesis; and (b) the cosine of the isolation angle, for the heavy-stable-charged-particle track candidates after the preselection, in the data (triangles with error bars) and the background simulation (histogram). Distributions of N_σ as a function of the charged particle momentum (c) in the data and (d) in the signal simulation with $m_{\tilde{g}} = 4$, 10 and 25 GeV/c^2.

4.3 Combined selection efficiency

The efficiencies of the combination of all (charged and neutral) R-hadron selections, weighted by the expected production fractions, are displayed in Fig. 5 as a function of the gluino mass for $P_{\tilde{g}g} = 0\%$, in each of the three different final states, $q\bar{q}R^0R^0$, $q\bar{q}R^\pm R^0$ and $q\bar{q}R^\pm R^\pm$. The total efficiency is maximal for gluino masses in the vicinity of 27 GeV/c^2, where it exceeds 50% (to be compared to 35% when $P_{\tilde{g}g} = 100\%$). No events were selected in the data by the charged hadron selection, with 0.7 events expected from standard model backgrounds, mostly from $e^+e^- \rightarrow q\bar{q}$.
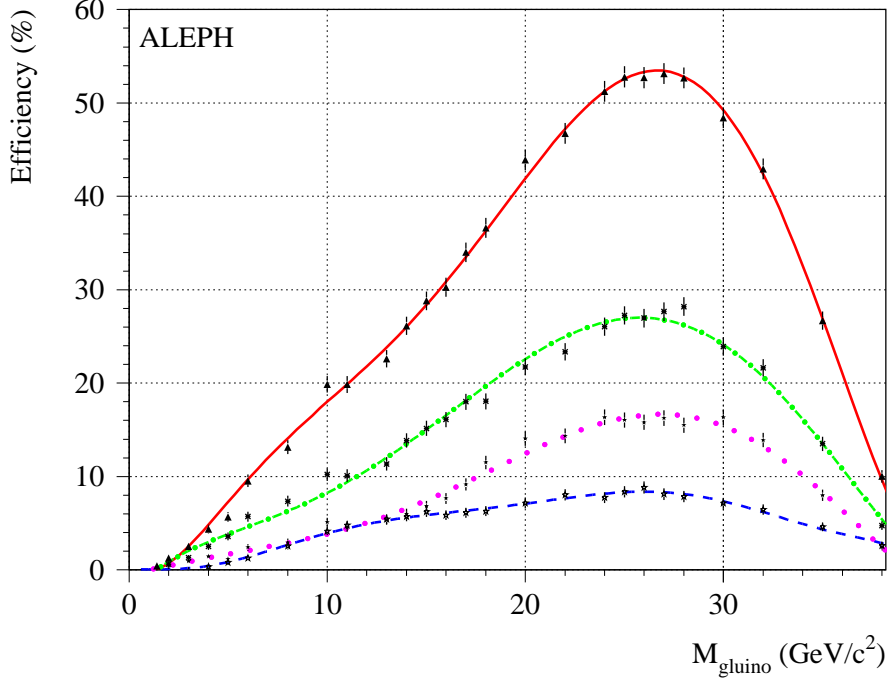
11

Figure 5: The $q\bar{q}\tilde{g}\tilde{g}$ selection efficiency as a function of the gluino mass, when $P_{\tilde{g}g} = 0\%$, for the $q\bar{q}R^0R^0$ final state (dashed curve), the $q\bar{q}R^\pm R^0$ final state (dot-dashed curve), the $q\bar{q}R^\pm R^\pm$ final state (dotted curve), and the sum of the three (full curve). The markers with error bars indicate the efficiencies obtained with each of the simulated samples, and the curves are obtained with a polynomial fit through these points.

4.4 Systematic uncertainties

Potentially large systematic uncertainties may arise from several sources and are listed below. Their relative effects on the number of signal events expected are given here for a gluino mass of $27\,\mathrm{GeV}/c^2$, but are similar for all masses.

- The hadronization is simulated with parton shower evolution, but the parton shower parameters are mostly unknown in the presence of gluinos. A variation of these parameters by $\pm100\%$ yields a $\pm3\%$ variation of the selection efficiency.

- The R-hadronic interaction cross section uncertainty of $\pm50\%$ changes the selection efficiency by $\pm9\%$ for $P_{\tilde{g}g} = 1$ and by $\pm3\%$ for $P_{\tilde{g}g} = 0$.

- The gluon constituent mass uncertainty yields an efficiency variation of $\pm2\%$ for $P_{\tilde{g}g} = 1$. The other gluino hadronization parameters of Section 3 have no sizeable effects.

- The uncertainty on $\alpha_S(m_Z) = 0.1183 \pm 0.0020$ turns into a variation of $\pm4\%$ of the production cross section.

- The QCD next-to-leading-order corrections to the cross section are at the percent level for gluino masses around $25\,\mathrm{GeV}/c^2$, and are included in the present estimate. The next-order corrections are not expected to have any visible effect.

The above uncertainties were taken into account according to Ref. [35].

12

4.5 Gluino mass limit

The number of $q\bar{q}\tilde{g}\tilde{g}$ events expected in the LEP 1 data is displayed in Fig. 6 as a function of the gluino mass, for $P_{\tilde{g}g}$ varying between 0 and 1. Altogether, when combined to the
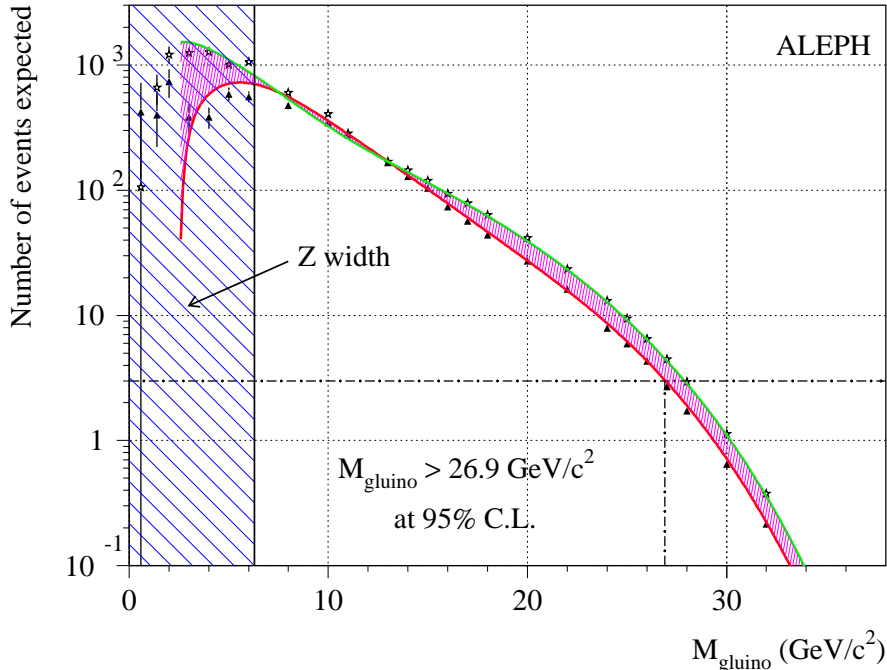

Figure 6: The number of $q\bar{q}\tilde{g}\tilde{g}$ events expected to be selected in the LEP 1 data by the neutral and charged R-hadron searches, as a function of the gluino mass, for $P_{\tilde{g}g}$ varying between 0 and 1 (shaded area). The markers with error bars (triangles for $P_{\tilde{g}g} = 1$, stars for $P_{\tilde{g}g} = 0$) show the individual values obtained from each of the simulated signal samples. Also shown is the region excluded by the Z lineshape measurement (hatched region), and the lower limit on the gluino-LSP mass (dot-dashed lines).

analysis of Ref. [17], this search results in a 95% C.L. absolute lower limit of $26.9\,\mathrm{GeV}/c^2$ on the mass of a gluino LSP (Fig. 6), which substantially improves the 2 to $18\,\mathrm{GeV}/c^2$ exclusion of Ref. [36] and exceeds the expectation from the study of Ref. [5].

5 Search for $q\bar{q}\tilde{q}\bar{\tilde{q}}$ with LEP 1 data

The same selections were applied with no modification to stable squark production through the $e^+e^- \rightarrow q\bar{q}\tilde{q}\bar{\tilde{q}}$ process. As shown in Fig. 1, the precise electroweak measurements allow all squark masses below $1.3\,\mathrm{GeV}/c^2$ to be excluded with the method of Ref. [17], irrespective of the squark decay and hadronization.

The number of events expected to be selected by the charged and neutral R-hadron searches described above is displayed in Fig. 7 for larger squark masses. This search results in a 95% C.L. lower limit of $15.7\,\mathrm{GeV}/c^2$ on the mass of a stable squark. The result was translated into upper limits on lifetimes, as presented in Fig. 8 for squarks and gluinos. Conservatively, the selection efficiency was assumed to vanish for neutral-R-hadron decays within the calorimeter volume, and for charged-R-hadron decays within the tracking volume. The scenario of Ref. [7] is excluded for sbottom lifetimes in excess of $1\,\mathrm{ns}$.
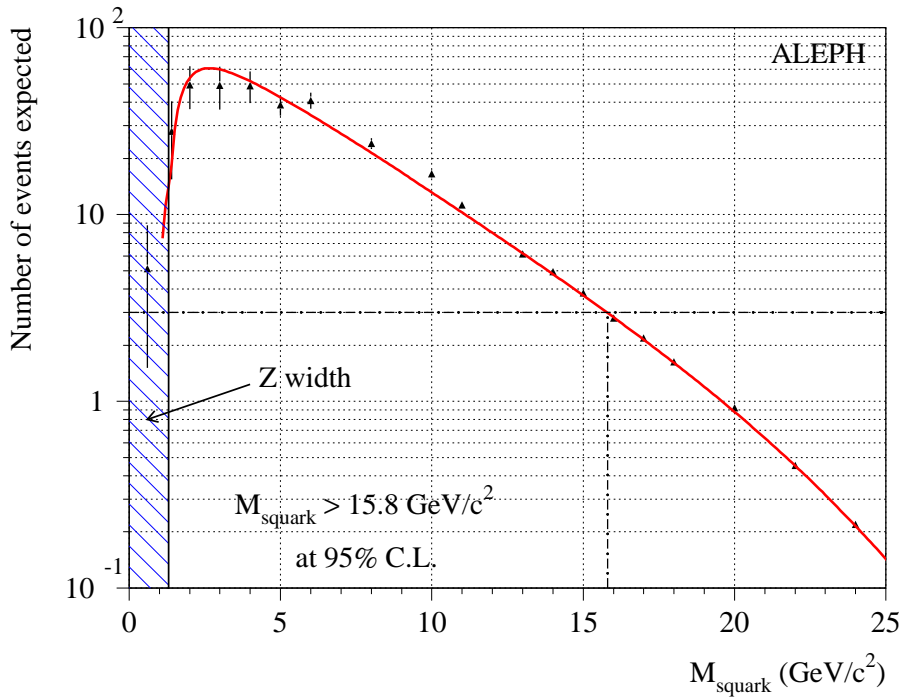
Figure 7: The number of $q\bar{q}\tilde{q}\bar{\tilde{q}}$ events expected to be selected in the LEP 1 data as a function of the squark mass (full curve). The triangles with error bars show the individual values obtained from each of the simulated signal samples. Also shown is the region excluded by the Z lineshape measurement (hatched region), and the lower limit on the squark-LSP mass (dot-dashed lines).

Figure 8: The upper limit on the squark and gluino lifetimes as a function of their mass (full curve). The hatched areas are excluded at more than 95% C.L.

6 Search for stable squarks in $e^+e^- \to \tilde{q}\bar{\tilde{q}}$ at LEP 2

If the lightest supersymmetric particle is a squark or, more generally, if the lightest squark does not decay within the detector volume, its pair production gives rise to a final state with two stable squark-R-hadrons, of which at least one is charged in a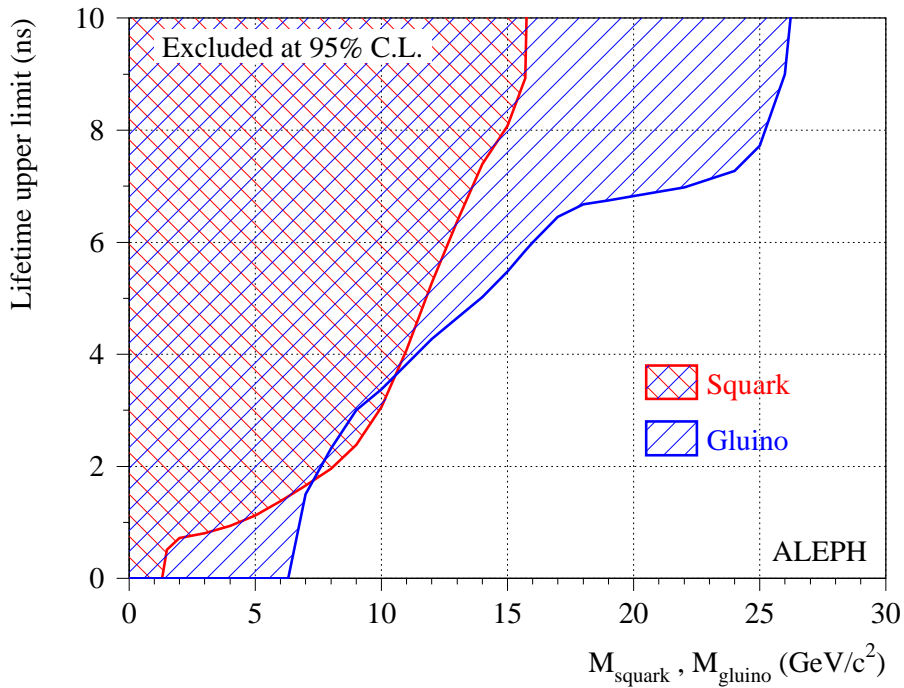t least 60% of the cases [3]. These charged R-hadrons can then be identified using the kinematic characteristics of squark-pair production and the large specific ionization dE/dx measured with the time projection chamber, as described in the previous section.

The stable stop search of Ref. [3] was extended to lower stop masses so as to provide an overlap with the search of Section 5, and to sbottom pair production. The production cross sections for stops and sbottoms, and the corresponding upper limits derived from the stable stop search, are shown in Fig. 9 for a vanishing coupling to the Z.
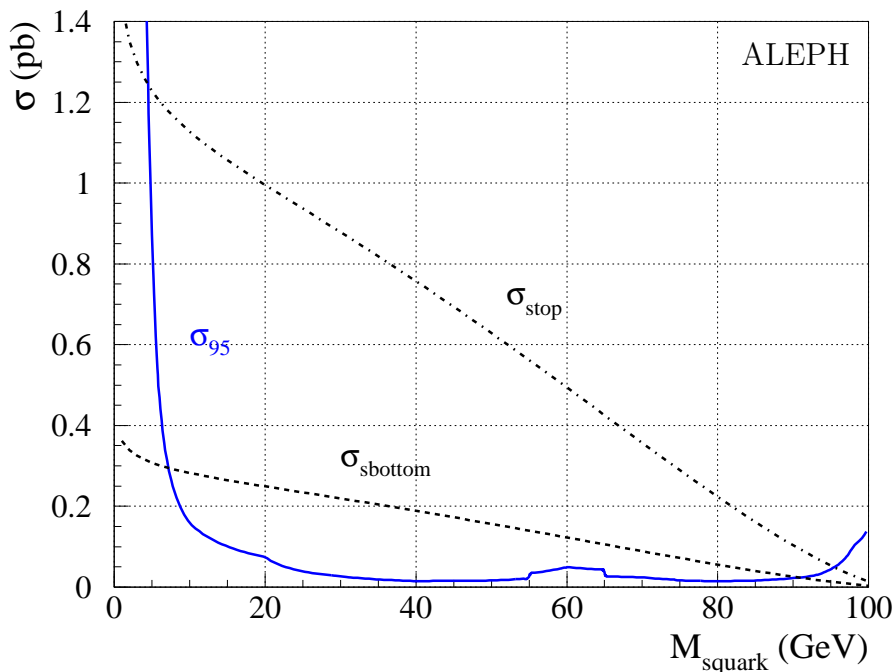
Figure 9: The production cross sections for $e^+e^- \to \tilde{t}\bar{\tilde{t}}$ and $\tilde{b}\bar{\tilde{b}}$ at $\sqrt{s} = 209\,\text{GeV}$, as a function of the squark mass. Also shown is the observed 95% C.L. upper limit on the cross section, derived from the stable stop search of Ref. [3].

This stable heavy charged particle search therefore allows stable stop masses between 5 and $95\,\text{GeV}/c^2$ and stable sbottom masses between 7 and $92\,\text{GeV}/c^2$ to be excluded at 95% C.L. When combined with the result of the search for $e^+e^- \to q\bar{q}\tilde{q}\bar{\tilde{q}}$ with LEP 1 data presented in the previous section, stable hadronizing squarks are excluded below $95\,\text{GeV}/c^2$ (up-squarks) and $92\,\text{GeV}/c^2$ (down-squarks).

7 Search for $e^+e^- \to \tilde{t}\bar{\tilde{t}} \to c\tilde{g}\bar{c}\tilde{g}$ at LEP 2

If the gluino is the LSP and the lighter stop quark the NLSP, the stop then decays into a gluino and a c or a u quark. The corresponding decay widths [22] are such that, for all

practical purposes, the stop quark is essentially stable if the mass difference ΔM between the stop-R-hadron and the gluino-R-hadron masses is smaller than the D mass, while it decays promptly if $\Delta M > m_D$, *i.e.*, when the $\tilde{t} \to c\tilde{g}$ decay channel is open. In the former case, the stable stop search of Section 6 applies here too with no modification. In the latter case, the final state topology is a pair of acoplanar jets from the $c\bar{c}$ hadronization accompanied by missing energy carried away by the mass of the two gluinos. The selection of this final state and its results are discussed in Section 7.1. The $\Delta M \simeq m_D$ case, in which the stop lifetime can take any value, is addressed in Section 7.2.

7.1 The case of prompt stop decays

7.1.1 Event selection

The discriminant variables listed below were designed for generic acoplanar jet topologies:

- the visible mass M_{vis} and energy E_{vis}, computed with all energy-flow particles;

- the energy E_{12} detected within 12° from the beam axis;

- the total energy carried by neutral hadrons, E_{NH};

- the energy of the most energetic lepton, E_ℓ;

- the energy in a 30° half-angle cone around the most energetic lepton, E_ℓ^{30};

- the energy computed without the identified leptons, E_{had};

- the energy measured in a 30° azimuthal wedge around the direction of the missing transverse momentum, E_{Wedge};

- the energy measured beyond 30° from the beam axis, E_{30};

- the momentum transverse to the beam axis, computed with all energy flow particles, p_T, without neutral hadrons, p_T^{exNH} and with good tracks only, p_T^{ch};

- the number of good tracks, N_{ch};

- the acoplanarity angle Φ_{acop}, between the directions of the momenta in the two event hemispheres, projected onto a plane perpendicular to the beam axis. Here, the hemispheres are defined with respect to a plane perpendicular to the thrust axis;

- the transverse acoplanarity angle, Φ_{acopT}, defined as above, but the hemispheres are now defined with respect to the transverse thrust axis, *i.e.*, the thrust axis of the event projected onto a plane perpendicular to the beam axis;

- the cosine of the polar angle of the missing momentum vector, $\cos\theta_{\text{miss}}$;

- the cosine of the polar angle of the thrust axis, $\cos\theta_{\text{T}}$;

- the event thrust T;

- the polar angle of the scattered electron, θ_{scat}, computed from the missing energy and momentum under the hypothesis that the event originates from a $\gamma\gamma$ interaction.

A preselection was used against two-photon events, characterized by their small visible energy and their boost along the beam direction. To reject these events, M_{vis} was required to exceed $15\,\mathrm{GeV}/c^2$, p_T to be larger than $2.5\%\sqrt{s}$ and N_{ch} to be in excess of 7. Moreover, the angles Φ_{acop} and Φ_{acopT} were both required to be smaller than $178.5°$, $\cos\theta_{\mathrm{miss}}$ and $\cos\theta_{\mathrm{T}}$ smaller than 0.85 and E_{12} smaller than $0.5\%\sqrt{s}$.

The distribution of the visible energy after this preselection is shown in Fig. 10 for the data, the background expected from different sources and the signal for two different values of ΔM. For events with small ΔM, only a small amount of energy is available for
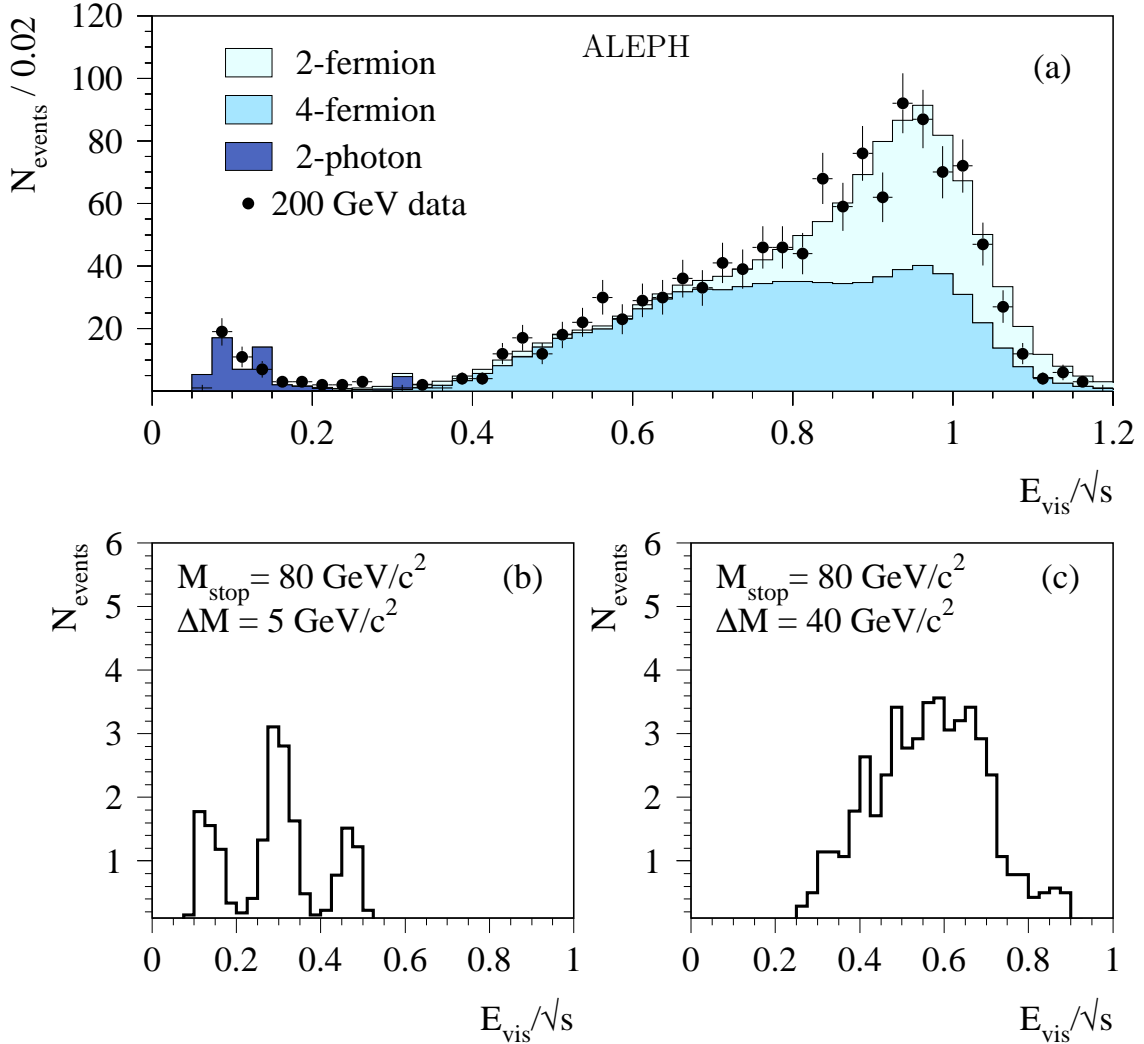
Figure 10: Distributions of the visible energy observed in the data at $\sqrt{s} = 200\,\mathrm{GeV}$ (dots with error bars) and expected from various background sources (shaded histograms), after the preselection cuts (a). The lower two plots show the expected distributions for the signal, with $\Delta M = 5\,\mathrm{GeV}/c^2$ (b) and $40\,\mathrm{GeV}/c^2$ (c). For small ΔM, the R-hadron composition is clearly visible: double-charged-R-hadrons events have largest visible energy, and double-neutral-R-hadrons events have smallest visible energy. For large ΔM, the three peaks are merged because of the broader visible energy distributions.

17

the recoiling c-quark system, which results in a small particle multiplicity and small visible energy. In addition, the R-hadrons tend to be emitted back to back, which turns into large values for thrust, acoplanarity and transverse acoplanarity. These characteristics are very similar to those of two-photon events. In contrast, events with large ΔM are characterized by large particle multiplicity and visible energy, and the background arises mainly from four-fermion production and q$\bar{\text{q}}$ events.

In fact, the distribution of most of the variables of the above list, and thus the relevant background sources, are strongly correlated with the value of ΔM. Three different selections were therefore developed for small, intermediate and large ΔM values.

The selection criteria follow closely those used for the squark searches in the case of a neutralino LSP, described in Ref. [37]. However, the values of the most relevant cuts were re-optimized with the $\bar{N}_{95}$ method (that minimizes the expected 95% C.L upper limit on the signal cross section [38]) to account for the reduced missing energy, the larger integrated luminosity and the centre-of-mass energy increase, and to include the subtraction of the four-fermion and q$\bar{\text{q}}$ backgrounds. The optimized cut values for the three selections are given in Table 2.

Table 2: Selection criteria for the search for R-hadrons from stop pair production in the acoplanar jet topology, in the three ΔM regions.

Variable	Small ΔM	Intermediate ΔM	Large ΔM
M_{vis}	$> 15\,\text{GeV}/c^2$	$> 15\,\text{GeV}/c^2$	$> 15\,\text{GeV}/c^2$
$p_T/\sqrt{s}$	$> 2.5\%$	$> 4\%$	$> 7.5\%$
N_{ch}	> 7	> 11	> 18
$E_{\text{vis}}/\sqrt{s}$	$< 50\%$	$< 70\%$	$< 80\%$
$E_{12}/\sqrt{s}$	$< 0.5\%$	$< 0.5\%$	$< 0.5\%$
$\cos\theta_{\text{miss}}$	> 0.8	> 0.8	> 0.8
$\cos\theta_{\text{T}}$	> 0.8	> 0.8	> 0.85
Φ_{acop}	$< 178.5°$	$< 176°$	$< 176°$
Φ_{acopT}	$> 178.5°$	$< 177°$	$< 177°$
$E_{\text{Wedge}}/\sqrt{s}$	$< 12.5\%$	$< 12.5\%$	$< 12.5\%$
T	<0.96	<0.94	<0.92
θ_{scat}	$> 5°$	$[6°, 80°]$	$[15°, 80°]$
p_T/E_{vis}	$-$	$> 12.5\%$	$> 12.5\%$
$p_T^{\text{ch}}/\sqrt{s}$	$> 1.5\%$	$-$	$-$
$p_T^{\text{exNH}}/\sqrt{s}$	$> 2\%$	$-$	$-$
E_{had}	$[10\,\text{GeV}, 40\%\sqrt{s}]$	$< 55\%\sqrt{s}$	$< 75\%\sqrt{s}$
$E_{\text{NH}}/\sqrt{s}$	$< 10\%$	$-$	$-$
$E_{\text{NH}}/E_{\text{vis}}$	$-$	$< 30\%$	$-$
$E_{\ell}/\sqrt{s}$	$> 20\%$	$-$	$-$
$E_{\ell}^{30}/\sqrt{s}$	$-$	$> 1\%$	$> 1\%$
E_{30}/E_{vis}	$-$	$-$	$> 80\%$

7.1.2 Selection efficiency

The selection efficiencies were obtained from simulated samples (Section 3.1.5) for over 150 different values of $(m_{\tilde{t}}, m_{\tilde{g}})$, and were then parametrized as a function of $m_{\tilde{t}}$ and $m_{\tilde{g}}$ with a polynomial function. For example, the efficiency of the three selections is shown in Fig. 11 for $m_{\tilde{t}} = 80 \, \text{GeV}/c^2$ as a function of the gluino mass. The ΔM intervals in which each of the three selections are to be used were again determined, as a function of the stop mass, with the $\bar{N}_{95}$ prescription. For example, for $m_{\tilde{t}} = 80 \, \text{GeV}/c^2$, the switching ΔM values are 16 and 33 GeV/c^2. These switching ΔM values tend to decrease with the stop mass.
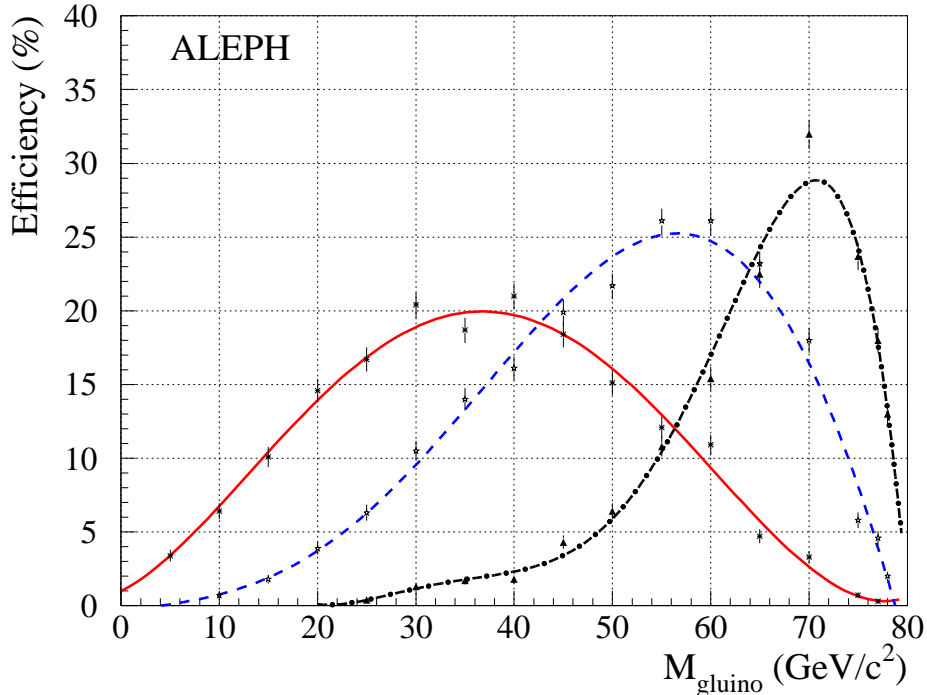

Figure 11: The three parametrized selection efficiencies for $m_{\tilde{t}} = 80 \, \text{GeV}/c^2$ (full curve, large ΔM selection; dashed curve, intermediate ΔM selection; and dot-dashed curve, small ΔM selection) as a function of $m_{\tilde{g}}$. The dots with error bars show the actual efficiencies obtained from the individual simulated samples.

7.1.3 Systematic uncertainties

The signal efficiencies may be affected by uncertainties in the simulation of the stop and gluino R-hadronization physics, uncertainties related to the detector response for R-hadrons and uncertainties due to the limited size of the simulated samples. Systematic effects from the physics assumptions were estimated by varying the free parameters of the simulation, as described in Section 3.

- The gluino-gluon bound state probability was assumed to be 10%. The effects of a probability variation from 0% to 100% depend on the stop and gluino masses. For light gluinos (around 30 GeV/c^2), the efficiency increases with $P_{\tilde{g}g}$, i.e., with

19

the fraction of R^0R^0 final states, as is the case for the LEP 1 neutral R-hadron selections (Section 4.1). Indeed, such light R-hadrons substantially interact in the calorimeters, and it is only when two neutral R-hadrons are present in the final state that the missing energy becomes large enough to make the present selection fully efficient. In contrast, for larger gluino masses and small mass differences, the two gluinos are produced approximately back to back with similar energies, and have almost no interaction in the calorimeters. This configuration leads to a cancellation in the measured missing transverse momentum in the R^0R^0 final state. In this case, the efficiency decreases when $P_{\tilde{g}\tilde{g}}$ increases. A map of the corresponding uncertainty (up to $\pm 20\%$ in extreme cases) was built in the $(m_{\tilde{t}},\, m_{\tilde{g}})$ plane.

- The R-hadronic interaction cross section uncertainty of $\pm 50\%$ changes the selection efficiency by at most $\pm 5\%$ in the small ΔM region, and by a negligible amount otherwise.

- The effective spectator mass uncertainty yields relative efficiency variations of $\pm 5\%$, $\pm 3\%$ and $\pm 3\%$ in the small, intermediate and large ΔM regions, respectively. The gluon constituent mass uncertainty has no visible effect.

- The uncertainty on the Peterson fragmentation parameter ϵ_b (varied here between 0.003 and 0.010) gives rise to an efficiency change of $\pm 8\%$, irrespective of the ΔM value.

The limited statistics of the 150 signal samples (1000 events each) and the parametrization of the efficiencies with a polynomial are responsible for 3% uncertainty. Beam-related backgrounds, which affect the determination of E_{12}, were not simulated. The effect on the selection efficiency, determined from events collected at random beam crossings, is a relative decrease of 5%.

Finally, uncertainties in the simulation of the background were assessed by comparing the effect of each cut separately on the data and on the simulated backgrounds after the preselection. The relative differences, although compatible with the uncertainty due to limited statistics, were conservatively added in quadrature, for a total possible deviation of 9%.

To derive the final result, all the above uncertainties were taken into account following the method of Ref. [35].

7.1.4 Results and interpretation

The numbers of candidate events observed in the data between 1997 and 2000 are displayed in Table 3. These numbers are in agreement with the numbers of events expected from standard model background sources.

In the framework of the MSSM with R-parity conservation, the outcome of this search can be translated into constraints in the $(m_{\tilde{t}}, m_{\tilde{g}})$ plane when the stop quark decays with a 100% branching fraction into a stable hadronizing gluino and a c quark. Regions excluded by this search at 95% C.L. are shown in Fig. 12, for $\theta_{\mathrm{mix}} = 56°$ and $0°$, corresponding to vanishing and maximal stop coupling to the Z, respectively.

Table 3: The numbers of candidate events observed in the data between 1997 and 2000, and the numbers of events expected from standard model background sources, for the small, intermediate and large ΔM selections.

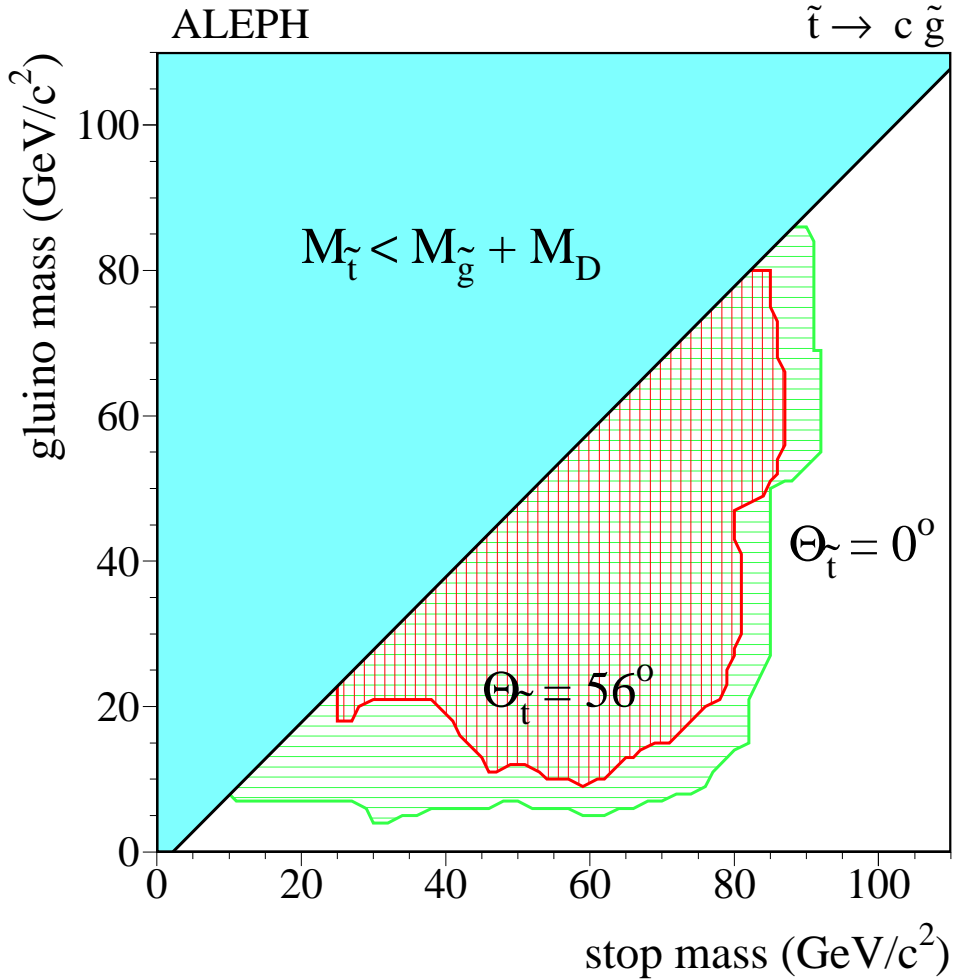| Year	Luminosity [pb^{-1}]	Small ΔM		Int. ΔM		Large ΔM	
		Obs.	Exp.	Obs.	Exp.	Obs	Exp.
2000	207.3	6	8.1	11	14.7	17	17.0
1999	236.9	9	8.7	15	16.7	19	19.5
1998	173.6	7	6.9	11	13.4	17	15.2
1997	56.8	1	2.2	5	4.4	4	5.0
Total	674.6	23	25.9	42	49.2	57	56.7

Figure 12: The 95 % C.L. excluded regions in the plane ($m_{\tilde{t}}$, $m_{\tilde{g}}$) from the acoplanar jet search at LEP 2, for maximal (horizontal hatching) and minimal (cross hatching) stop coupling to the Z. The shaded area corresponds to a stable stop and is not accessible to this search.

7.2 The $\Delta M \simeq m_{\mathrm{D}}$ case

The analyses of Sections 6 and 7.1 do not suffice to efficiently cover the $\Delta M = m_{\mathrm{D}}$ line: along this line, the phase space for the $\tilde{\mathrm{t}} \to \mathrm{c}\tilde{\mathrm{g}}$ decay is so small that the stop lifetime may take any intermediate value, for which none of the previous selections is fully effective.

Stop pair production followed by decays into $\mathrm{c}\tilde{\mathrm{g}}$ was simulated for $\Delta M = m_{\mathrm{D}}$ as explained in Section 3, with stop proper decay lengths varying from $1\,\mathrm{mm}$ to $1\,\mathrm{m}$. The acoplanar jet search of Section 7.1, the search for heavy stable charged particles of Section 6 and the search for kinks and secondary vertices of Ref. [3] were applied in turn to these simulated samples. Altogether, they allow all stop masses between 14 and $80\,\mathrm{GeV}/c^2$ to be excluded for this very small mass difference, irrespective of the stop lifetime, for a vanishing stop coupling to the Z.

8 Combined results

As can be seen from Fig. 12, no absolute stop mass limit can be extracted from the results of the acoplanar jet plus missing energy search alone. An absolute mass limit is obtained by combining all searches presented in this paper in the following way.

- Small gluino masses do not give rise to large enough missing energy to be addressed by the $\tilde{\mathrm{t}} \to \mathrm{c}\tilde{\mathrm{g}}$ search. However, the searches for $\mathrm{e}^+\mathrm{e}^- \to \mathrm{q}\bar{\mathrm{q}}\tilde{\mathrm{g}}\tilde{\mathrm{g}}$ at LEP 1 presented in Ref. [17] and in Section 4 allow all gluino masses below $26.9\,\mathrm{GeV}/c^2$ to be excluded when the gluino is the LSP ($m_{\tilde{\mathrm{g}}} < m_{\tilde{\mathrm{t}}}$).

- Stable stops, *i.e.*, with $\Delta M < m_{\mathrm{D}}$, are excluded up to $15.7\,\mathrm{GeV}/c^2$ with the search for $\mathrm{e}^+\mathrm{e}^- \to \mathrm{q}\bar{\mathrm{q}}\tilde{\mathrm{q}}\tilde{\bar{\mathrm{q}}}$ at LEP 1 presented in Section 5, and up to $95\,\mathrm{GeV}/c^2$ by the search for heavy stable charged particles presented in Section 6.

- Promptly decaying heavy stops, *i.e.*, with $\Delta M > m_{\mathrm{D}}$, are excluded up to masses of $85\,\mathrm{GeV}/c^2$ by the acoplanar jet search of Section 7.1.

- For $\Delta M \simeq m_{\mathrm{D}}$, masses up to $80\,\mathrm{GeV}/c^2$ are excluded independently of the stop lifetime, as mentioned in Section 7.2.

The result of the combination is displayed in Fig. 13. All stop masses below $80\,\mathrm{GeV}/c^2$ are excluded at 95% C.L. when either the stop or the gluino is the lightest supersymmetric particle. When combined with the result of Ref. [2], all stop masses below $63\,\mathrm{GeV}/c^2$ are excluded irrespective of the nature of the LSP.

Sbottom quarks were also searched for, but the acoplanar jet search proved not to be efficient enough to cope with *(i)* the four times smaller cross section of $\mathrm{e}^+\mathrm{e}^- \to \tilde{\mathrm{b}}\bar{\tilde{\mathrm{b}}} \to \mathrm{b}\bar{\mathrm{b}}\tilde{\mathrm{g}}\tilde{\mathrm{g}}$, even when b-tagging is applied to reduce the background; and *(ii)* the very small mass differences (down to m_{K}) for which the sbottom may decay promptly to $\mathrm{s}\tilde{\mathrm{g}}$. However, the Z lineshape limits and the excluded areas (1), (2) and (3) of Fig. 13 apply as well for all squark species, and in particular for the sbottom. All sbottom masses below $27.4\,\mathrm{GeV}/c^2$ are therefore excluded at 95% C.L. when either the sbottom or the gluino is the lightest supersymmetric particle.
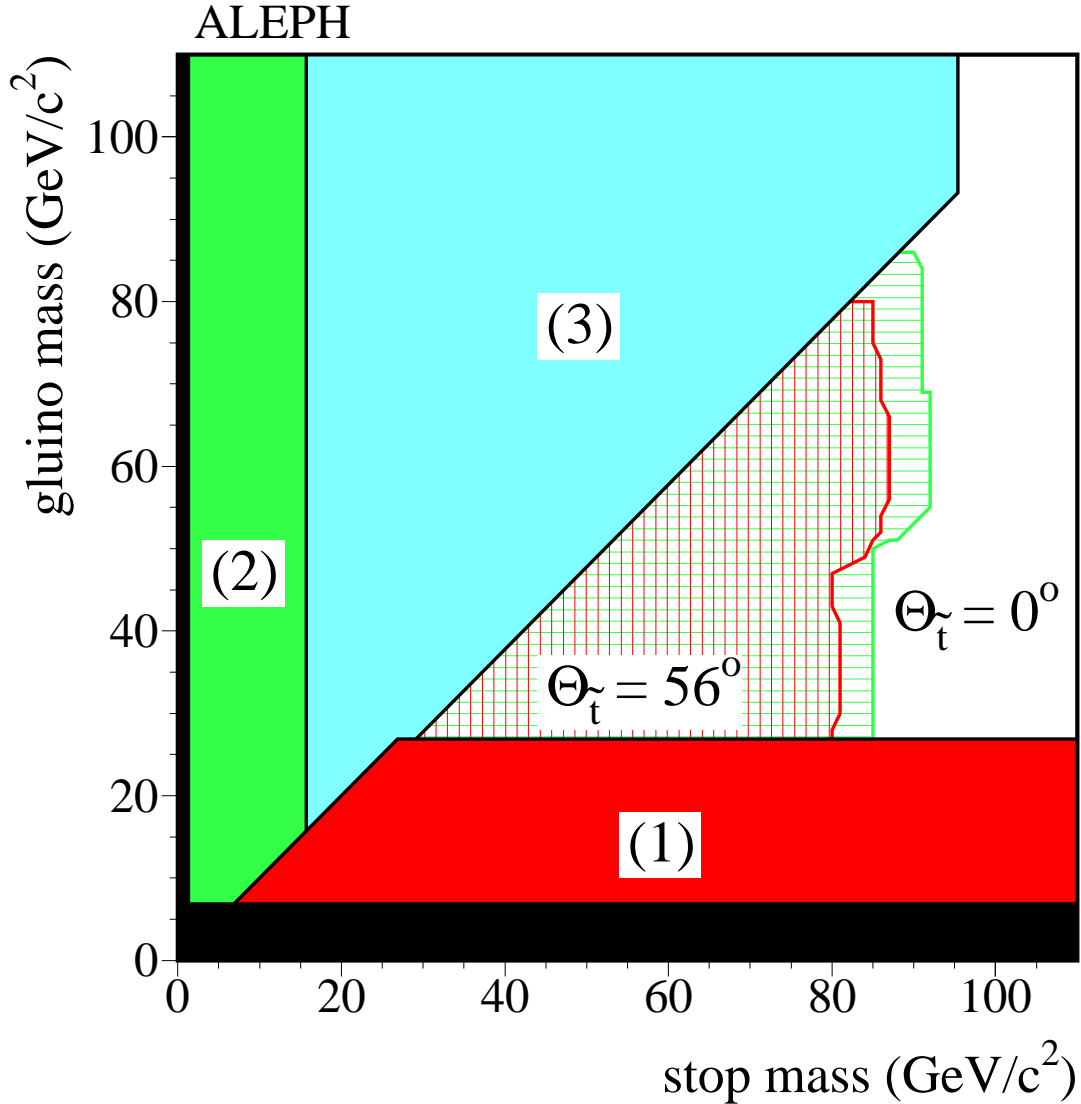
Figure 13: The 95% C.L. excluded regions in the plane $(m_{\tilde{t}}, m_{\tilde{g}})$ from the combination of all searches presented in this paper. The black area at very small gluino and squark masses is excluded by the precise measurement of the Z lineshape; Regions (1), (2) and (3) are excluded by the search for $e^+e^- \to q\bar{q}\tilde{g}\tilde{g}$ at LEP 1, for $e^+e^- \to q\bar{q}\tilde{q}\bar{\tilde{q}}$ at LEP 1, and for heavy stable charged particles from $\tilde{q}\bar{\tilde{q}}$ production at LEP 2, respectively. The hatched areas are excluded by the acoplanar jet with missing energy search at LEP 2.

9 Conclusions

Searches for stable, hadronizing squarks and gluinos have been performed with the data collected at centre-of-mass energies from 88 to 209 GeV by the ALEPH detector at LEP. No evidence for such a signal was observed in any of the production processes studied: $e^+e^- \to q\bar{q}\tilde{g}\tilde{g}$, $e^+e^- \to q\bar{q}\tilde{q}\bar{\tilde{q}}$ and $e^+e^- \to \tilde{q}\bar{\tilde{q}}$. The following absolute mass limits were obtained at the 95% confidence level in the framework of the MSSM with R-parity conservation:

- a gluino LSP is excluded for $m_{\tilde{g}} < 26.9\,\mathrm{GeV}/c^2$;

- a down-type squark LSP is excluded for $m_{\tilde{q}} < 92\,\mathrm{GeV}/c^2$;

- an up-type squark LSP is excluded for $m_{\tilde{q}} < 95\,\mathrm{GeV}/c^2$;

- a sbottom quark NSLP is excluded up to masses of $27.4\,\mathrm{GeV}/c^2$ if the LSP is a gluino;

- a stop quark NSLP is excluded up to masses of $80\,\mathrm{GeV}/c^2$ if the LSP is a gluino, and up to masses of $63\,\mathrm{GeV}/c^2$ irrespective of the nature of the LSP.

The above squark and gluino LSP limits also apply in any supersymmetric model in which squarks or gluinos are long-lived. In particular, the scenario of Ref. [7] with a gluino of 12 to $16\,\mathrm{GeV}/c^2$ decaying into a b quark and a long-lived sbottom with a mass of 2 to $5\,\mathrm{GeV}/c^2$ is no longer viable.

The results presented in this paper improve on related existing results [36, 39]. In particular, absolute lower limits on the masses of stable squarks, stable gluinos, and stop quarks decaying into stable gluinos, have been reported for the first time.

10   Acknowledgements

References

[1] J. Ellis and S. Rudaz, *Phys. Lett.* **B 128** (1983) 248;
M. Drees and K.I. Hikasa, *Phys. Lett.* **B 252** (1990) 127.

[2] The ALEPH Coll., *"Search for scalar quarks in e^+e^- collisions at $\sqrt{s}$ up to 209 GeV"*, *Phys. Lett.* **B 537** (2002) 5.

[3] The ALEPH Coll., *"Search for a scalar top almost degenerate with the lightest neutralino in e^+e^- collisions at $\sqrt{s}$ up to 202 GeV"*, *Phys. Lett.* **B 488** (2000) 234.

[4] H.P. Nilles, *Phys. Rept.* **110** (1984) 1;
H.E. Haber and G.L. Kane, *Phys. Rept.* **117** (1985) 75;
R. Barbieri, *Riv. Nuovo Cim.* **11N4** (1988) 1.

[5] H. Baer, K. Cheung and J.F. Gunion, *Phys. Rev.* **D 59** (1999) 075002, and references therein.

[6] J. Ellis et al., *Nucl. Phys.* **B 238** (1984) 453.

[7] E.L. Berger et al., *Phys. Rev. Lett.* **86** (2001) 4231.

[8] G.R. Farrar and P. Fayet, *Phys. Lett.* **B 76** (1978) 575.

[9] The ALEPH Coll., *"ALEPH: a detector for electron-positron annihilations at LEP"*, *Nucl. Instrum. and Methods* **A 294** (1990) 121.

[10] The ALEPH Coll., *"Performance of the ALEPH detector at LEP"*, *Nucl. Instrum. and Methods* **A 360** (1995) 481.

[11] T. Sjöstrand et al, *"High-energy-physics event generation with PYTHIA 6.1"*, *Comput. Phys. Commun.* **135** (2001) 238.

[12] F.A. Berends and R. Kleiss, *Nucl. Phys.* **B 260** (1985) 32.

[13] P. Verdier, *"Recherche des squarks et des gluinos dans l'expérience DELPHI au LEP"*, PhD Thesis, unpublished.

[14] A.H. Hoang, M. Jeżabek, J.H. Kühn and T. Teubner, *Phys. Lett.* **B 338** (1994) 330.

[15] M.H. Seymour, *Nucl. Phys.* **B 436** (1995) 163.

[16] See for instance: C.-W. Chiang, Z. Luo and J.L. Rosner, *"Light gluino and the running of α_S"*, hep-ph/0207235.

[17] P. Janot, *"The light gluino mass window revisited"*, CERN-EP/2003-004, to be published in *Phys. Lett.* **B**.

[18] T. Sjöstrand, private communication;
See also `http://www.thep.lu.se/~torbjorn/Pythia.html`.

[19] E. Norrbin and T. Sjöstrand, *Nucl. Phys.* **B 603** (2001) 297.

[20] C. Peterson, D. Schlatter, I. Schmitt and P.M. Zerwas, *Phys. Rev.* **D 27** (1983) 105.

[21] I.G. Knowles and T. Sjöstrand, *"QCD event generators"*, in Workshop on Physics at LEP 2, CERN, Geneva, Switzerland, 2-3 Feb 1995.

[22] K. Hikasa and M. Kobayashi, *Phys. Rev.* **D 36** (1987) 724.

[23] G. Altarelli et al., *Nucl. Phys.* **B 208** (1982) 365.

[24] A. Mafi and S. Raby, *Phys. Rev.* **D 62** (2000) 035003.

[25] G. Altarelli, private communication.

[26] M.R. Pennington, *"Glueballs: The naked truth"*, hep-ph/9811276.

[27] S. Jadach, W. Placzek and B.F.L. Ward, *Phys. Lett.* **B 390** (1997) 298.

[28] S. Jadach, B.F.L. Ward and Z. Was, *Comput. Phys. Commun.* **79** (1994) 503.

[29] J.A.M. Vermaseren, *"Two gamma physics versus one gamma physics and whatever lies in between"*, Presented at Gamma-Gamma Workshop, Amiens, France, Apr 8-12, 1980;
The ALEPH Coll., *"An Experimental study of $\gamma\gamma \to$ hadrons at LEP"*, Phys. Lett. **B 313** (1993) 509.

[30] S. Jadach et al., *Comput. Phys. Commun.* **119** (1999) 272.

[31] J. Fujimoto, *Comput. Phys. Commun.* **100** (1997) 128.

[32] T. Sjöstrand, *Comput. Phys. Commun.* **82** (1994) 74.

[33] The ALEPH Coll., *"Mass limit for the standard model Higgs boson with the full LEP 1 ALEPH data sample"*, Phys. Lett. **B 384** (1996) 427.

[34] The ALEPH Coll., *"Search for scalar top quarks in e^+e^- collisions at LEP 1 energies"*, Contribution EPS-0416 to the international Europhysics Conference on High Energy Physics, Brussels, Belgium, July 27-August 2, 1995.

[35] R.D. Cousins and W.L Highland, *Nucl. Instrum. and Methods* **A 320** (1992) 331.

[36] The DELPHI Coll., *"Search for an LSP gluino at LEP with the DELPHI detector"*, Eur. Phys. J. **C 26** (2003) 505.

[37] The ALEPH Coll., *"Searches for scalar top and scalar bottom quarks at LEP 2"*, Phys. Lett. **B 413** (1997) 431.

[38] The ALEPH Coll., *"Search for the standard model Higgs boson"*, Phys. Lett. **B 313** (1993) 299;
J.F. Grivaz and F. Le Diberder, *"Complementary analyses and acceptance optimization in new particle searches"*, LAL **92-37** (1992).

[39] The DELPHI Coll., *"A search for heavy stable and longlived squarks and sleptons in e^+e^- collisions at energies from $130\,GeV$ to $183\,GeV$"*, Phys. Lett. **B 444** (1998) 491.